

Modelling attosecond probing of electron wavepacket dynamics in non-aligned molecules

J Schmidt¹, E Goulielmakis² and V S Yakovlev¹

¹ Department of Physics, Ludwig-Maximilians-Universität München, Am Coulombwall 1, D-85748 Garching, Germany

² Max-Planck-Institut für Quantenoptik, Hans-Kopfermann-Str. 1, D-85748 Garching, Germany

E-mail: Vladislav.Yakovlev@physik.uni-muenchen.de

Received 29 November 2007, in final form 22 April 2008

Published 20 May 2008

Online at stacks.iop.org/JPhysB/41/115602

Abstract

We propose and simulate an attosecond pump–probe scheme applied to an ensemble of non-aligned (or partially aligned) diatomic molecules. Non-dissociative dynamics initiated by an ultraviolet pump pulse are probed by photoionizing the molecule with an attosecond extreme-ultraviolet probe pulse. Photoelectron spectra recorded for different delays between the pulses exhibit signatures of streaking and sub-femtosecond quantum beating. If more than one vibrational state is excited, the nuclear motion modulates the visibility of quantum interference effects.

(Some figures in this article are in colour only in the electronic version)

1. Introduction

Recent progress in laser technology and the generation of attosecond ($1 \text{ as} = 10^{-18} \text{ s}$) light pulses [1–4] has opened possibilities to make time-resolved measurements of electron and nuclear dynamics in molecules with an unprecedented time resolution. Such dynamical processes are typically induced by a few-cycle laser pulse with a precisely controlled electric field, including its carrier-envelope-offset phase (CEP). In some cases, valuable conclusions regarding a molecule's behaviour on the attosecond time scale can be made without employing attosecond pulses. As a few important examples, we mention probing molecular dynamics by electron recollision based on either measurements of the kinetic energies of molecular fragments [5, 6], or on observations of molecular high harmonics [7], the control of electron localization by a few-cycle infrared pulse [8] and the observation of quantum interference of vibrational wavepackets using a pair of CEP-stabilized few-cycle laser pulses [9]. However, the most direct and versatile method to observe attosecond dynamics would be to use the pump–probe technique, with a pump pulse capable of triggering an ultrafast electronic process and with a probe pulse capable of capturing the ensuing dynamics.

First experiments of this kind in isolated atoms include the Auger decay triggered by an attosecond light pulse and probed by an infrared laser field [10] or electron tunnelling in atoms probed by an attosecond pulse [11]. Furthermore, a series of theoretical investigations of electron dynamics in atoms holds promise for exciting experiments once the appropriate technologies become available [12, 13].

Study of ultrafast electron dynamics in molecules comprises yet another exciting research area that falls within the scope of attosecond science and aims at both the investigation of fundamental aspects of hyperfast electron motion in a molecule [14, 15], as well as the exploration of possibilities for steering this motion with precisely controlled light fields giving rise to angstrom-scale molecular electronics [4]. To the best of our knowledge, attosecond pump–probe experiments on molecules have not been reported so far, but several theoretical studies of relevant phenomena have already been published [13, 14, 16, 17].

The photoionization of an aligned diatomic molecule prepared in a superposition of two different electronic states was investigated in [14, 16, 17]. If the spectral width of the photoionizing pulse exceeds the separation between the two energy levels, the measured electron spectra strongly depend on the delay between the excitation and the photoionization.

It was found that important information about electron motion can be extracted from asymmetries in photoelectron angular distributions.

Another approach to measure molecular dynamics with attosecond resolution is to dissociate a molecule with an attosecond pulse [13]. In this case, the nuclear wavepacket can be reconstructed from the kinetic energies of the ions produced as a result of the Coulomb explosion that follows the photoionization.

The most straightforward way to electronically excite a molecule is resonant absorption of light with an the appropriate photon energy. For the vast majority of molecules, this can be realized with sources residing spectrally in the near or deep ultraviolet, whilst atoms would need photons in the vacuum-ultraviolet range. Here, we propose and model a scheme in which a pump pulse in the deep ultraviolet is used to create an electronic wavepacket in a molecule, and a soft-x-ray attosecond pulse probes the launched dynamics. Our approach enables access into molecular electron dynamics based on the current ‘state of art’ of attosecond tools and technologies that have recently become available [18, 19].

In the aforementioned theoretical investigations, molecules were modelled with nuclei being fixed in space. That is, molecules were assumed to be perfectly aligned, and the nuclear motion was neglected. This was the price of employing advanced numerical and analytical tools to model fast electron dynamics. In the present paper, we approach the problem from a different side: we use a fairly simple model to describe electron dynamics, but we let the molecule vibrate, and we show how to adapt conventional models that describe angular distributions of photoelectrons to model attosecond pump–probe experiments on non-aligned or partially aligned molecular ensembles.

2. The model

The theoretical description of pump–probe photoionization of diatomic molecules has a long history. Pioneering contributions of Seel and Domcke [20] followed by more than a decade of research aimed at modelling the photoionization in the field of two intense light pulses. However, the physical situation that we consider in our paper is a different one: the photoionizing pulse is a rather weak extreme-ultraviolet (XUV) pulse with a duration on the attosecond time scale. As a pump pulse, we consider an ultraviolet (UV) pulse of a moderate intensity, sufficient to excite molecules, but weak enough to prevent photoionizing or dissociating them. To describe this physical situation, which we believe to be relevant to the forthcoming attosecond pump–probe experiments on molecules, we propose a model that may be regarded as a generalization of streaking models developed for attosecond experiments on isolated atoms [21].

Photoelectron spectra, created by an XUV pulse and measured in dependence on the delay to a laser pulse, carry important information about the electron and nuclear dynamics. Especially interesting is the case where the two pulses overlap, so that an attosecond electron wavepacket is launched by an XUV pulse in the presence of a laser field. In

this case, the field interacts with the wavepacket, recording information about its time structure in the photoelectron spectra. This effect is referred to as attosecond streaking [22], and it was shown that the wavepacket can be fully reconstructed from a series of spectra measured for different delays between the laser and XUV pulses [23, 24]. While the most basic application of this technique is the characterization of attosecond light pulses, the method itself allows us to measure the properties of any coherent electron wavepacket of a duration smaller or comparable to the period of the streaking field [25].

There are a few assumptions serving as a basis for our model. The assumption of moderate laser intensities allows us to describe the molecular wavefunction in the field of a laser (UV) pulse as a linear combination of stationary bound states with time-dependent coefficients. We also neglect the role of the electron and nuclear spins, assuming that the interaction with the spins can be neglected on the short time scales considered here and that the bandwidth of the probe (XUV) pulse is much larger than the energy splitting caused by the interaction. Henceforth, atomic units ($e = \hbar = m_e = 1$) will be used unless stated otherwise.

With the above assumptions, the stationary molecular states can be represented in the Born–Oppenheimer approximation as

$$|\Psi_{n,v,N,M,\Lambda}\rangle = \sqrt{\frac{2N+1}{8\pi^2}} \Phi_n(\mathbf{r}', R) \chi_{n,v}(R) \mathcal{D}_{M\Lambda}^N(\hat{R}), \quad (1)$$

where \mathbf{r}' is the electron position in the molecule-fixed frame, \mathbf{R} is the vector from nucleus 1 to nucleus 2, $\Phi_n(\mathbf{r}', R)$ specifies the n th electronic state, $\chi_{n,v}(R)$ is the nuclear wavefunction of the v th vibrational state on the n th electronic surface and N is the total angular momentum of the molecule, excluding the electron and nuclear spins. Projections of \mathbf{N} on the z -axis of the lab frame and on the inter-nuclear axis are denoted as M and Λ , respectively. The rotational part of wavefunction (1) is given by the rotation matrix $\mathcal{D}_{M\Lambda}^N(\hat{R})$, and the factor $\sqrt{(2N+1)/8\pi^2}$ ensures the normalization $\langle \Psi_{n,v,N,M,\Lambda} | \Psi_{n,v,N,M,\Lambda} \rangle = 1$, provided that the vibrational eigenstates are normalized by $\int_0^\infty R^2 |\chi_{n,v}(R)|^2 dR = 1$.

For the wavefunction of a photoionized molecule, we use the following ansatz:

$$|\Psi\rangle = \int d^3\mathbf{p} |\phi_{\mathbf{p}}\rangle \sum_{v,N,M,\Lambda} a_{\mathbf{p},v,N,M,\Lambda} |\Psi_{v,N,M,\Lambda}^{\text{ion}}\rangle, \quad (2)$$

where $|\phi_{\mathbf{p}}\rangle$ is a single-electron continuum state that corresponds to an outgoing wave with a momentum \mathbf{p} in the laboratory frame, and the bound states of the molecular ion are given by

$$|\Psi_{v,N,M,\Lambda}^{\text{ion}}\rangle = \sqrt{\frac{2N+1}{8\pi^2}} \chi_v^{\text{ion}}(R) \mathcal{D}_{M\Lambda}^N(\hat{R}). \quad (3)$$

The probability amplitudes $a_{\mathbf{p},v,N,M,\Lambda}$ determine the measured photoelectron spectra

$$\sigma(\mathbf{p}) = \langle \Psi | \phi_{\mathbf{p}} \rangle \langle \phi_{\mathbf{p}} | \Psi \rangle = \sum_{v,N,M,\Lambda} |a_{\mathbf{p},v,N,M,\Lambda}|^2. \quad (4)$$

This relation simply means that contributions from ionization channels that result in different final states of the molecular ion must be added incoherently.

To obtain an expression for the probability amplitudes $a_{\mathbf{p},v,N,M,\Lambda}$, we first separate the Hamiltonian $\hat{H}(t)$ into two parts,

$$\hat{H}(t) = \hat{H}_L(t) + \hat{V}_{XUV}(t), \quad (5)$$

where $\hat{H}_L(t)$ includes the molecular Hamiltonian and the interaction with a laser field (the UV pump pulse), while $\hat{V}_{XUV}(t)$ describes the interaction with an attosecond XUV pulse. The time-evolution operator of the total Hamiltonian $\hat{H}(t)$ satisfies the Dyson equation [26]

$$\hat{U}(t, t_0) = \hat{U}_L(t, t_0) - i \int_{t_0}^t dt' \hat{U}(t, t') \hat{V}_{XUV}(t') \hat{U}_L(t', t_0), \quad (6)$$

where \hat{U}_L is the propagator that corresponds to the operator $\hat{H}_L(t)$ and t_0 is a moment of time preceding the interaction with external fields. The probability amplitude of ionizing the molecule and observing a free electron with a momentum \mathbf{p} is given by

$$a_{\mathbf{p},v,N,M,\Lambda} = \lim_{t \rightarrow \infty} \langle \Psi | \hat{U}(t, t_0) | \Psi(t_0) \rangle,$$

where $\Psi(t_0)$ describes the initial state of the molecule. If the laser field is too weak to ionize the molecule on its own, then $\langle \Psi | \hat{U}_L(t, t_0) | \Psi(t_0) \rangle = 0$, and without any further approximations we obtain

$$a_{\mathbf{p},v,N,M,\Lambda} = -i \int_{t_0}^{\infty} dt \langle \phi_{\mathbf{p}} | \langle \Psi_{v,N,M,\Lambda}^{\text{ion}} | \hat{U}(\infty, t) \times \hat{V}_{XUV}(t) \hat{U}_L(t, t_0) | \Psi(t_0) \rangle \rangle, \quad (7)$$

which is a standard S -matrix expression for the probability amplitude except the fact that, in our case, the laser field affects the electron dynamics before *and* after the moment of photoionization.

The transition operator $\hat{V}_{XUV}(t)$, written in the length gauge within the dipole approximation, reads as

$$\hat{V}_{XUV}(t) = (\mathbf{r} \hat{\mathbf{e}}_{XUV}) \left(\frac{1}{2} \mathcal{E}_{XUV}(t - \tau) e^{-i(t-\tau)\Omega} + \text{c.c.} \right), \quad (8)$$

where the XUV pulse is assumed to be linearly polarized along the vector $\hat{\mathbf{e}}_{XUV}$, Ω is the central frequency of the pulse and τ is the delay of the XUV pulse with respect to the pump pulse.

In the presence of a moderately strong laser field, the molecular wavefunction can be expressed as a linear combination of stationary bound states,

$$\hat{U}_L(t, t_0) | \Psi(t_0) \rangle = \sum_{n,v,N,M,\Lambda} c_{n,v,N,M,\Lambda}(t) e^{-itE_{n,v,N,\Lambda}} \times | \Psi_{n,v,N,M,\Lambda} \rangle, \quad (9)$$

where $E_{n,v,N,\Lambda}$ is the energy of the state $| \Psi_{n,v,N,M,\Lambda} \rangle$. The initial state of the molecule is given by the probability amplitudes $c_{n,v,N,M,\Lambda}(t_0)$. Ansatz (9) implies that the laser field does not dissociate the molecule.

The evaluation of the full propagator \hat{U} calls for approximations. In this paper, we adopt the so-called strong-field approximation: we neglect the interaction of a free electron with its parent ion. In spite of its name, this approximation is not limited to the strong-field ionization—the main condition imposed by this approximation is that once an electron is set free, it should quickly leave the vicinity of the

ion. While there are known drawbacks of this approximation, it was demonstrated to correctly predict electron spectra in streaking experiments [2, 27–29], as long as the photon energy of the XUV pulse significantly exceeded the ionization potential, and the intensity of the laser field is moderate, so that the photoelectron never returns to its parent ion.

In addition to the strong-field approximation, we neglect the XUV field in the propagator \hat{U} , which means that only a single XUV photon can be absorbed by an electron. With these approximations, the single-electron continuum in a homogeneous electric field is given by the Volkov states, which, in the length gauge and coordinate representation, take the form

$$| \phi_{\mathbf{p}}(t) \rangle = | \mathbf{p} + \mathbf{A}_L(t) \rangle \exp \left(-\frac{i}{2} \int_{t_0}^t [\mathbf{p} + \mathbf{A}_L(t')]^2 dt' \right), \quad (10)$$

where $| \mathbf{p} \rangle = \exp(i\mathbf{p}\mathbf{r})$, and

$$\mathbf{A}_L(t) = \int_{-\infty}^t \mathbf{E}_L(t') dt' \quad (11)$$

is the vector potential of the laser field $\mathbf{E}_L(t)$ (this definition of the vector potential is traditionally used in attosecond streaking models, although it differs from the conventional definition by a factor equal to the vacuum speed of light). Before and after the laser pulse, when $\mathbf{A}_L = 0$, the Volkov states become usual plane waves.

It is known that the Coulomb interaction of a free electron with its parent ion may significantly distort the angular distributions of photoelectrons for atoms [30], as well as those for aligned molecules [31, 32]. While it is possible to account for this interaction using the Coulomb-eikonal Volkov [30] or the two-centre Coulomb–Volkov [33] wavefunctions for $| \phi_{\mathbf{p}} \rangle$, this would significantly complicate our theory. Since the primary goal of this paper is to describe attosecond probing beyond the approximation of frozen nuclei, we chose to keep the description of the electron dynamics possibly simple. So we do not consider angular electron distributions in the present paper, which would require a straightforward but complex extension of the theory; instead, we focus our attention on electron spectra measured in a certain fixed direction.

Describing the free-electron dynamics with the Volkov states, we obtain

$$\langle \phi_{\mathbf{p}} | \langle \Psi_{v^+,N^+,M^+,\Lambda^+}^{\text{ion}} | \hat{U}(t, t') \approx \exp \left(-\frac{i}{2} \int_{t'}^t [\mathbf{p} + \mathbf{A}_L(t'')]^2 dt'' \right) \times e^{-i(t-t')E_{v^+,N^+,M^+,\Lambda^+}^{\text{ion}}} \langle \mathbf{p} + \mathbf{A}_L(t') | \langle \Psi_{v^+,N^+,M^+,\Lambda^+}^{\text{ion}} |, \quad (12)$$

where $E_{v^+,N^+,M^+,\Lambda^+}^{\text{ion}}$ is the energy of a molecular ion state $| \Psi_{v^+,N^+,M^+,\Lambda^+}^{\text{ion}} \rangle$.

For brevity, the indices n, v, N, M and Λ , describing a stationary state of a neutral molecule, will be denoted by a single symbol \wp , while the indices v^+, N^+, M^+ and Λ^+ , describing a state of a molecular ion, will be denoted by \wp^+ . To obtain the final expression for the probability amplitude $a_{\wp^+}(\tau, \mathbf{p})$, we use approximation (12) together with (8) and (9), apply the rotating-wave approximation (RWA) for the XUV pulse (but not for the UV one), omit insignificant phase factors and take the limits $t_0 \rightarrow -\infty, t \rightarrow \infty$, which yields

$$a_{\wp^+}(\tau, \mathbf{p}) = -\frac{i}{2} \sum_{\wp} \int_{-\infty}^{\infty} dt \mathcal{E}_{XUV}(t - \tau) \times c_{\wp}(t) e^{i\varphi_{\wp,\wp^+}(t,\mathbf{p})} V_{\wp,\wp^+}(\mathbf{p} + \mathbf{A}_L(t)). \quad (13)$$

Here, we collected all the phase terms into

$$\varphi_{\wp, \wp^+}(t, \mathbf{p}) = \left(\frac{p^2}{2} + E_{\wp^+}^{\text{ion}} - E_{\wp} - \Omega \right) t - \int_t^\infty \left[\mathbf{p} \mathbf{A}_L(t') + \frac{A_L^2(t')}{2} \right] dt', \quad (14)$$

and introduced the bound-free transition matrix element defined as

$$V_{\wp, \wp^+}(\mathbf{p}) = \langle \mathbf{p} | \langle \Psi_{\wp^+}^{\text{ion}} | (\mathbf{r} \hat{\mathbf{e}}_{\text{XUV}}) | \Psi_{\wp} \rangle. \quad (15)$$

An explicit expression for this matrix element, as well as the details regarding the evaluation of $c_{\wp}(t)$, are given in appendix A.

So far, we assumed a molecule in a pure quantum-mechanical state. In most cases, however, one has to deal with an incoherent mixture of pure states by describing the initial state with a density matrix [34]. To calculate photoelectron spectra in this case, one should first evaluate probability amplitudes (13) for each pure state in the initial ensemble and then combine them using the elements of the density matrix as weight coefficients. If the initial density matrix is diagonal, that is, if it represents a completely incoherent superposition of states, this procedure simply means evaluating spectra (4) for different initial states and then adding them together,

$$\sigma(\tau, \mathbf{p}) = \sum_{\wp_0} P_{\wp_0} \sigma_{\wp_0}(\tau, \mathbf{p}) = \sum_{\wp_0} P_{\wp_0} \sum_{\wp^+} |a_{\wp^+, \wp_0}(\tau, \mathbf{p})|^2, \quad (16)$$

where $\wp_0 = \{n_0, v_0, N_0, M_0, \Lambda_0\}$ denotes all possible states in the initial ensemble and P_{\wp_0} stands for the probabilities of these states. In particular, in a non-aligned ensemble of molecules, all allowed values of the projection of the total angular momentum on the z -axis (M_0) must have equal probabilities.

Electron spectra are usually plotted as functions of the electron energy $\epsilon = p^2/2$ rather than momentum. For a given direction of observation, the probability density of observing an electron with an energy ϵ is given by $I(\epsilon) = (2\epsilon)^{-1/2} \sigma(\sqrt{2\epsilon})$, where the pre-factor is required to satisfy $I(\epsilon) d\epsilon = \sigma(p) dp$.

3. Simulations

We applied our theory to study the UV-pump XUV-probe photoionization of an ensemble of non-aligned nitric oxide (NO) molecules. We chose nitric oxide mainly due to the accessibility of published spectroscopic data and that of theoretical models describing the molecule. However, the principles developed here are expected to be fully applicable to any molecule that does not dissociate once it is photoionized or electronically excited. For the NO molecule, the energy difference between the ground state $X^2\Pi$ and the first excited electronic state $A^2\Sigma$ amounts to $\hbar\omega_{12} = 5.45$ eV, while the ionization potential for the ground state is 9.26 eV [35]. The photon energy of the UV pulse was chosen to photoexcite the molecules through a single-photon absorption. The dipole transition from the $X^2\Pi$ to the $A^2\Sigma$ state can be viewed

as an excitation of the outer electron from the π^* HOMO to the σ^* LUMO. The transition matrix element is rather small (0.0895 au [36, 37]), but the possibility to excite the molecule with near-UV light, for which sources of intense femtosecond (fs) pulses residing in the required spectral range have recently become available [38], makes this molecule a possible candidate for forthcoming attosecond experiments.

We assumed that, initially, all molecules are in the electronic and vibrational ground state (at room temperature, only 0.01% of the molecules are in vibrationally excited states). To speed up our simulations, we also assumed that the initial ensemble of molecules is rotationally cold (on the femtosecond time scale, the rotational motion can safely be neglected; the inclusion of the rotation in the initial ensemble would only affect the angular distribution of photoelectrons, which is out of the scope of the present paper).

Depending on the bandwidth of the UV pulse, one or more vibrational states can be populated upon the photoexcitation to the $A^2\Sigma$ state (the Franck–Condon factors for the first three vibrational states are equal to 0.12, 0.32 and 0.34, respectively [39]). This creates a vibrational wavepacket with an oscillation period of 14.0 fs [35]. Further details can be found in appendix A. The rest of this section is devoted to the results of our simulations.

We first present simulations in which the pump pulse was a linearly-polarized bandwidth-limited UV pulse with a Gaussian temporal profile and a full width at half maximum (FWHM) of 100 fs. The bandwidth of this pulse is smaller than the separation between any two vibrational states of an electronically-excited molecule (150 versus 2400 cm^{-1} [35]), so that only one of these states can be populated by the pulse. With a central wavelength of 227.5 nm, tuned to the transition to the lowest vibrational state of $A^2\Sigma$ and a peak intensity of 10^{11} W cm^{-2} , the pulse excites merely 3.6% of the molecules. Even though it is possible to increase the excitation probability by increasing the laser intensity, we decided to keep it at a level where the electron dynamics can be accurately modelled in a basis consisting of just a few bound states. At larger intensities, the photoionization by the UV pulse cannot be neglected, and our simple description of the bound electron dynamics (9) ceases to be valid. Nevertheless, this constraint should not be regarded as a limitation for experiments, where the upper boundary on the laser intensity is set by the requirement that the excited electronic state should not be depleted by the laser pulse. Furthermore, since the methods developed here are not limited to diatomic molecules, systems with a substantially higher photoionization cross-section might be considered for experiments. As a probe pulse, we employed a linearly-polarized bandwidth-limited 150 attosecond XUV pulse with a central photon energy of 91 eV. Both pulses were polarized in the direction towards the detector.

In figure 1, we show the results of these simulations for two delay ranges. The first spectrogram (figure 1(a)) was calculated for overlapping UV and XUV pulses, where the dominant effect was streaking [22]: a photoelectron launched in the presence of the UV field can be either accelerated or decelerated by the field, depending on the photoionization moment. As a result, the photoelectron

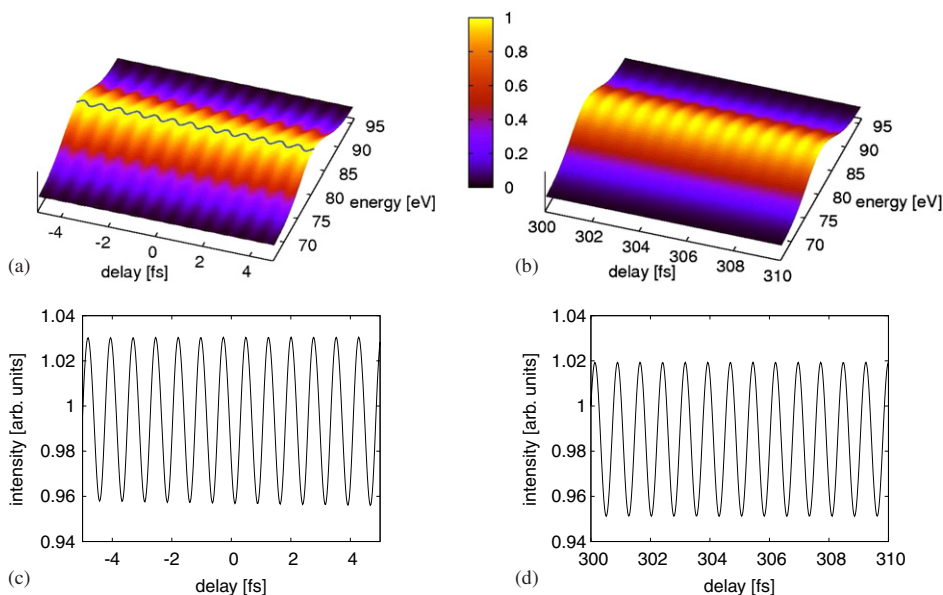


Figure 1. Pump–probe photoionization with a 100 fs UV and a 0.15 fs XUV pulses. The spectrograms in panels (a) and (b) show the dependence of the electron spectra on the delay between the two pulses: (a) for overlapping and (b) for non-overlapping pulses. For the zero delay, the XUV pulse arrives at the peak intensity of the UV pulse. For positive delays, the UV pulse precedes the XUV one. The oscillating curve in panel (a) highlights the peaks of the spectra, elucidating the streaking effect. Panels (c) and (d) show slices of the spectrograms at a photoelectron energy of 83.7 eV.

spectra are broadened and shifted to either smaller or larger kinetic energies, depending on the delay between the UV and XUV pulses. For the parameters that we used, the amplitude of the spectral shift was 0.5 eV.

The second spectrogram (figure 1(b)) was recorded with an XUV pulse being significantly delayed with respect to the UV one. In this case, the so-called quantum beats are observed, the origin of which is further clarified by figure 2: the spectral FWHM of the XUV pulse is equal to 12 eV, which is significantly larger than the energy difference $\hbar\omega_{12}$ between the first two electronic states of the molecule. Therefore, the contributions from these two states to the photoelectron spectra overlap and interfere with each other. Whether this interference is constructive or destructive it is determined by the relative difference in phases of these contributions, which depends on the delay.

Panels (c) and (d) in figure 1 show slices of the spectrograms made at an electron energy for which the amplitude of the quantum beats is maximal. This energy is 83.7 eV, just above the centre of the peak associated with the $X^2\Pi$ state. In the streaking region, the intensity grows when the spectrum is shifted towards higher energies, and it decreases when the shift is opposite. Consequently, the intensity oscillates with the period of the UV carrier wave. Since we matched the central frequency of the UV pulse to the transition frequency, this period is equal to the period of quantum beats in figure 1(d): $2\pi/\omega_{12} = 31.4\text{au} = 760$ attosecond.

The next series of simulations was performed with a UV pulse as short as 5 fs, the other parameters being identical to those of the previous simulation. The spectra were recorded in the polarization direction of the XUV pulse (the

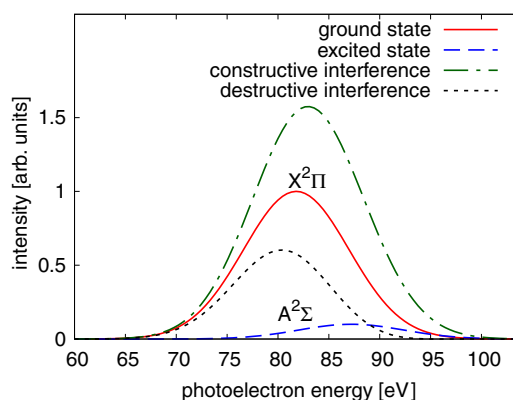


Figure 2. Quantum interference in photoelectron spectra. When the XUV pulse ionizes a coherent superposition of the $X^2\Pi$ and $A^2\Sigma$ states, the photoelectron spectrum depends on the relative phase between the states. In our simulations, the individual contributions from these states are centred at 81.8 eV and 87.2 eV, respectively.

photoelectron yield was maximal in this direction). The short duration of the UV pulse brings a new physical effect into play: a vibrational wavepacket is formed. However, this comes at a price, as the photoexcitation probability is only 0.013%. While an experimental observation of time-dependent quantum interferences would probably be difficult in this case, we present the results as an illustration of an effect that can potentially be observed in another system (a molecule with a larger photoexcitation cross-section) under more realistic conditions (larger laser intensities).

In figures 3(a) and (b), we plot the simulated spectrograms in two overlapping delay ranges: in the first one, from -8 fs

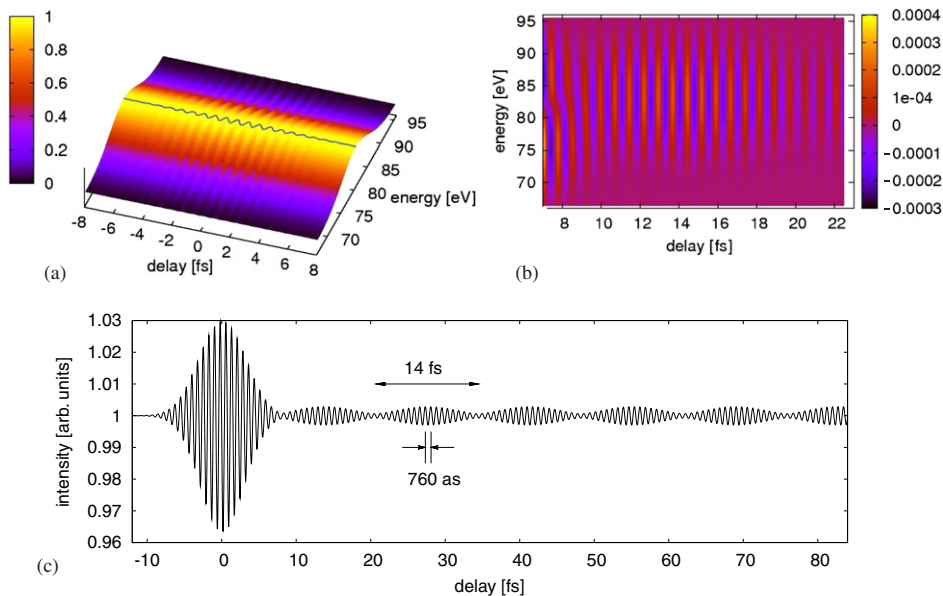


Figure 3. Simulation of a pump–probe measurement with a 5 fs UV and a 0.15 fs XUV pulses, polarized in the direction of observation. In panel (a), we plotted streaked photoelectron spectra, while panel (b) shows the difference between the pump–probe spectra and the contribution from the ground molecular state. The curve on the surface in panel (a) is a guide to the eye laid through the peaks of the spectra. The spectral intensity at 87.2 eV as a function of the delay is shown in panel (c). The nuclear motion leads to ‘revivals’ in quantum beating.

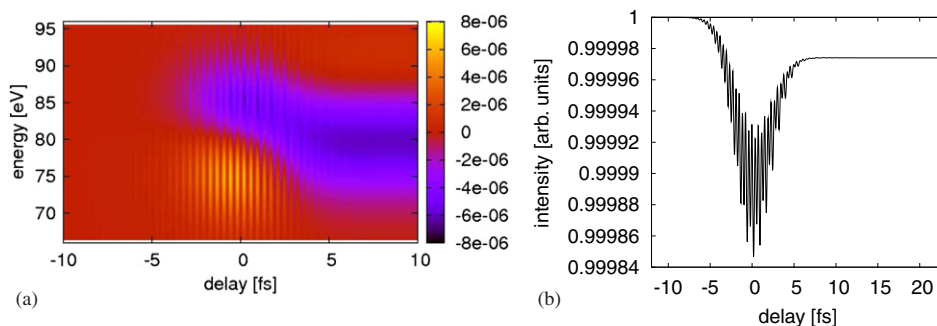


Figure 4. Simulation of a pump–probe measurement with orthogonally polarized 5 fs UV and 0.15 fs XUV pulses. Photoelectron spectra are recorded in the direction of the XUV polarization. Panel (a) depicts delay-dependent changes in photoelectron spectra with respect to the UV-free spectrum. Panel (b) contains a slice at 87.2 eV.

to 8 fs, streaking dominates over quantum beating, while the second delay range depicts a transition into a regime where quantum beating determines the delay dependence of the spectra.

Since the excitation probability is so small, we chose a different way to visualize the quantum beats in figure 3(b): from each spectrum, we subtracted the photoelectron spectrum obtained in the absence of the UV pulse. Figure 3(c) is analogous to figure 1(c)—it is a slice of the spectrogram at the photoelectron energy for which the quantum beats are strongest. In contrast to the results obtained with the 100 fs UV pulse, the amplitude of the quantum beats exhibits a slow modulation with a period of 14.0 fs, which matches the vibrational period of the electronically excited molecule. The maximal amplitude of the quantum beats is observed when all the photoelectron wavepackets launched from different vibrational $A^2\Sigma$ states have similar phases. At other delays,

when the contributions are dephased, the amplitude of the intensity oscillations is strongly reduced.

We found that, for a given direction of observation, quantum beats are not always observed, even if a coherent superposition of two electronic states is probed by a sufficiently broadband XUV pulse. This is illustrated in figure 4. We changed only one parameter with respect to the previous simulation: we polarized the pulses orthogonally to each other and recorded the photoelectron spectra in the polarization direction of the XUV pulse. Surprisingly, no quantum beating was observed in this geometry, even though a more detailed analysis showed that both the $X^2\Pi$ and $A^2\Sigma$ states contributed to the photoelectron spectrum. Precisely, after the interaction with the UV pulse, the ratio of the overall photoionization probability from the excited states to that from the ground state was equal to 2.3×10^{-5} , which is close to the probability ratio 2.8×10^{-5} observed in the geometry with parallel

polarizations, where quantum beating is evident (figure 3(c)). A selection rule responsible for the disappearance of quantum beats is explained in appendix B. Briefly, this is a consequence of two facts: (i) quantum interference can only be observed between channels that lead to the same final state of the quantum system and (ii) if the polarizations of the pump and probe pulses are orthogonal, then in each pair of states that could interfere with each other, only one state can be photoionized in the polarization direction of the XUV pulse.

Figure 4 also shows a very weak streaking effect. When the XUV pulse overlaps with an orthogonally polarized UV pulse (delays around zero in figure 4), the \mathbf{pA}_L term in (14) vanishes, and the spectral shifts due to the remaining $A_L^2(t)/2$ term are as small as 10^{-3} eV. Additionally, the UV field deflects electrons, so that the observed electron flux changes owing to the angular dependence of the photoionization probability.

4. Conclusions

In this paper, we presented a new model that we believe to be useful for the interpretation of forthcoming attosecond pump–probe experiments on molecules in which the electron spectra are observed in dependence on the delay between the pump and the probe. This model does not assume frozen nuclei, and it is applicable to the case where the same laser field populates excited states and serves as a streaking field for XUV-photoionized electrons. In simulations of a UV-pump XUV-probe measurement on an ensemble of non-aligned diatomic molecules, we clarified the role of nuclear dynamics and demonstrated a non-trivial selection rule that leads to the disappearance of quantum beating under certain conditions. We only considered attosecond probing of a coherent superposition of two bound electronic states, prepared by a UV pulse of a moderate intensity, but it is straightforward to generalize our approach to a broader class of phenomena where the approximation of frozen nuclei cannot be used. In particular, the simultaneous excitation of several electronic states with an intense broadband UV pulse may create an electron wavepacket with non-trivial dynamics [15]. These dynamics can be probed by an attosecond XUV pulse, and the interpretation of such measurements will require further development of theoretical tools, possibly based on the ideas presented in this paper.

Acknowledgments

Supported by the DFG Cluster of Excellence: Munich-Centre for Advanced Photonics. EG acknowledges a Marie-Curie fellowship (MEIF-CT-2005-02440) and a Marie-Curie Reintegration grant (MERG-CT-2007-208643). The authors acknowledge numerous helpful discussions with F Krausz, M Fieß and W Fuß.

Appendix A

In section 2, we derived general expressions for photoelectron spectra (16) in a UV-pump XUV-probe experiment. Here, we

extend that theoretical description with equations that we used to simulate the bound electron dynamics and to evaluate the transition matrix elements.

Equation (9) provides a general description of the photoexcitation by a UV pulse followed by a field-free evolution of the involved states. Collecting, once again, all the quantum numbers describing a certain molecular state into a single symbol \wp , we rewrite (9) as

$$\hat{U}_L(t, t_0)|\Psi(t_0)\rangle = \sum_{\wp} c_{\wp}(t) e^{-iE_{\wp}t} |\Psi_{\wp}\rangle. \quad (\text{A.1})$$

Initially, $c_{\wp}(t_0) = 0$ for all combinations of the indices n, v, N, M and Λ except a single combination \wp_0 , which describes a particular pure state belonging to the initial ensemble. For each such state, we calculated the time-dependent probability amplitudes $c_{\wp}(t)$ by numerically solving the following standard system of differential equations:

$$\frac{dc_{\wp}}{dt} = -i \sum_{\wp'} c_{\wp'}(t) V_{\wp, \wp'} e^{-i(E_{\wp'} - E_{\wp})t} \text{Re}[\mathcal{E}_L(t) e^{-i\omega_L t}], \quad (\text{A.2})$$

where $\mathcal{E}_L(t)$ and ω_L are the envelope and the central frequency of the laser (UV) pulse, and $V_{\wp, \wp'}$ is a matrix element for the transition between the bound states \wp' and \wp .

In this matrix element, the integration over angular variables can be performed analytically. The result is usually expressed using $3j$ symbols [40],

$$V_{\wp, \wp'} = \sqrt{\frac{4}{3}\pi} \sqrt{2N+1} \sqrt{2N'+1} \sum_{s, s_0=-1}^1 a_{s_0} (-1)^{s_0-s+M'-\Lambda'} \times \begin{pmatrix} N' & 1 & N \\ -M' & -s_0 & M \end{pmatrix} \begin{pmatrix} N' & 1 & N \\ -\Lambda' & -s & \Lambda \end{pmatrix} \overline{r_{s, \wp, \wp'}}. \quad (\text{A.3})$$

Here, the index s_0 and the factors a_{s_0} define the laser polarization: the derivation of (A.3) is based on expressing the dipole operator in spherical harmonics,

$$(\hat{\mathbf{r}}\hat{\mathbf{e}}_{UV}) = \sqrt{\frac{4}{3}\pi} \sum_{s_0=-1}^1 a_{s_0} Y_{1, s_0}(\hat{\mathbf{r}}). \quad (\text{A.4})$$

For a laser field linearly polarized along the z -axis, $a_0 = 1$ and $a_{\pm 1} = 0$, while for the x -polarization, $a_0 = 0$ and $a_{\pm 1} = \mp 2^{-1/2}$.

In equation (A.3), the term $\overline{r_{s, \wp, \wp'}}$ represents the part of the transition matrix element which stems from the integration over the inter-nuclear distance R and the electron coordinates $\hat{\mathbf{r}}'$ in a frame bound to the molecular axis,

$$\overline{r_{s, \wp, \wp'}} = \int dR \chi_{n, v}^*(R) \chi_{n', v'}(R) \int d\mathbf{r}' \Phi_{\wp}^*(\mathbf{r}', R) \times r' Y_{1s}(\hat{\mathbf{r}}') \Phi_{\wp'}(\mathbf{r}', R). \quad (\text{A.5})$$

Here, $\Phi_{\wp}(\mathbf{r}', R)$ stands for electron wavefunctions, which we evaluated in the LCAO approximation using the STO-3G basis set from [41].

In a similar way, the bound-free matrix element (15) for an XUV field polarized along the z -axis can be written

as [40, 42]

$$V_{\wp, \wp^+}(\mathbf{p}) = \frac{\sqrt{2N+1}\sqrt{2N'+1}}{2^{1/2}\pi^{3/2}} \sum_{s=-1}^1 \sum_{l=0}^{\infty} i^{-l} (-1)^{M-\Lambda} \\ \times Y_{l, M^+ - M}(\hat{\mathbf{p}}) \overline{r_{s, l, s-\Lambda, n, v, v^+}}(p) \sum_j \left[(2j+1) \right. \\ \times \begin{pmatrix} l & 1 & j \\ M^+ - M & 0 & M - M^+ \end{pmatrix} \begin{pmatrix} l & 1 & j \\ s - \Lambda & -s & \Lambda \end{pmatrix} \\ \left. \times \begin{pmatrix} N^+ & N & j \\ -M^+ & M & M^+ - M \end{pmatrix} \begin{pmatrix} N^+ & N & j \\ 0 & \Lambda & -\Lambda \end{pmatrix} \right]. \quad (\text{A.6})$$

Here, the index j takes all the values allowed by the 3 j symbols, and the $\overline{r_{s, l, s-\Lambda, n, v, v^+}}(p)$ results from the integration over the electron coordinates and the inter-nuclear distance,

$$\overline{r_{s, l, m, n, v, v^+}}(p) = \int_0^{\infty} dR [\chi_{v^+}^{\text{ion}}(R)]^* \chi_{n, v}(R) r_{s, l, m, n}(p, R), \\ \text{where} \quad (\text{A.7})$$

$$r_{s, l, m, n}(p, R) = \int d^3 \mathbf{r}' r'_j j_l(pr') Y_{1s}(\hat{\mathbf{r}}') Y_{lm}^*(\hat{\mathbf{r}}') \Phi_n(\mathbf{r}', R). \quad (\text{A.8})$$

In this paper, we completely neglect the role of the electron spin. To correctly describe angular distributions of photoelectrons, it may be necessary to include the spin into the model. This would be a straightforward procedure: the molecular states would be described by a few additional spin-related quantum numbers, and a more general expression for bound-free element can be found, for example, in [43].

Even though the formalism presented here is applicable to rotating molecules, for simplicity, we assumed that the initial ensemble was rotationally cold. In this case, the total angular momentum (excluding spin) N of an NO molecule in its ground state is equal to 1. With the degeneracy $\Lambda = \pm 1$, the initial molecular state is represented by an ensemble consisting of six rotational states. Upon photoexcitation into the $A^2\Sigma$ state, $\Lambda' = 0$ and N' may take any value between 0 and 2. So in order to describe the three vibrational states of an excited molecule, we needed 81 combinations of the quantum numbers N , M and Λ . The matrix element (A.3) allows transitions to infinitely many states \wp^+ of the ionized molecule. However, the transition probability decreases quickly with the angular momentum of the molecular ion N^+ . We found, that including N^+ larger than 8 did not significantly affect our simulation results. Altogether, in order to calculate one-electron spectrum given by (16), we had to sum over 42 000 channels determined by combinations of different initial, intermediate and final states.

Appendix B

In this appendix, we explain the selection rule responsible for the disappearance of quantum beating when photoelectrons are observed along the z -axis, which is also the polarization direction of the XUV pulse, while the laser field is polarized

in the xy plane. For the chosen observation direction, the non-zero terms in (A.6) are those for which $M = M^+$ (because $Y_{lm}(\theta = 0, \varphi) \equiv 0$ for non-zero m). That is, the total angular momenta of the neutral molecule and the molecular ion must have the same projection on the z -axis. Let us consider a superposition of two molecular states: a ground state $\wp_1 = \{n_1, v_1, N_1, M_1, \Lambda_1\}$ and a photoexcited state $\wp_2 = \{n_2, v_2, N_2, M_2, \Lambda_2\}$. Since quantum interference only takes place if \wp^+ is the same for both channels, the condition $M_1 = M_2$ must be satisfied, in order to observe quantum beats in spectra measured along the z -axis. At the same time, the selection rules encoded in (A.3) require that $M_2 = M_1 \pm 1$ if the UV pulse is polarized perpendicularly to the z -axis. Therefore, the quantum beats disappear in this geometry, even though $V_{\wp, \wp^+}(\mathbf{p} \parallel \hat{\mathbf{z}})$ has non-zero terms for the ground state, as well as for the photoexcited state.

References

- [1] Hentschel M, Kienberger R, Spielmann Ch, Reider G A, Milosevic N, Brabec T, Corkum P, Heinzmann U, Drescher M and Krausz F 2001 *Nature* **414** 509–13
- [2] Kienberger R *et al* 2004 *Nature* **427** 817–21
- [3] Corkum P B and Krausz F 2007 *Nature Phys.* **3** 381–7
- [4] Goulielmakis E, Yakovlev V S, Cavalieri A L, Uiberacker M, Pervak V, Apolonski A, Kienberger R, Kleineberg U and Krausz F 2007 *Science* **317** 769–75
- [5] Niikura H, Légaré F, Hasbani R, Bandrauk A D, Ivanov M Yu, Villeneuve D M and Corkum P B 2002 *Nature* **417** 917–22
- [6] Niikura H, Légaré F, Hasbani R, Ivanov M Yu, Villeneuve D M and Corkum P B 2003 *Nature* **421** 826–9
- [7] Baker S, Robinson J S, Haworth C A, Teng H, Smith R A, Chirilă C C, Lein M, Tisch J W G and Marangos J P 2006 *Science* **312** 424–7
- [8] Kling M F *et al* 2006 *Science* **312** 246–8
- [9] Ohmori K, Katsuki H, Chiba H, Honda M, Hagihara Y, Fujiwara K, Sato Y and Ueda K 2006 *Phys. Rev. Lett.* **96** 093002
- [10] Drescher M, Hentschel M, Kienberger R, Uiberacker M, Yakovlev V, Scrinzi A, Westerwalbesloh Th, Kleineberg U, Heinzmann U and Krausz F 2002 *Nature* **419** 803–7
- [11] Uiberacker M *et al* 2007 *Nature* **446** 627–32
- [12] Hu S X and Collins L A 2006 *Phys. Rev. Lett.* **96** 073004
- [13] Lin C D, Tong X M and Morishita T 2006 *J. Phys. B: At. Mol. Opt. Phys.* **39** S419–26
- [14] Chelkowski S, Yudin G L and Bandrauk A D 2006 *J. Phys. B: At. Mol. Opt. Phys.* **39** S409–17
- [15] Remacle F, Nest M and Levine R D 2007 *Phys. Rev. Lett.* **99** 183902
- [16] Yudin G L, Chelkowski S, Itatani J, Bandrauk A D and Corkum P B 2005 *Phys. Rev. A* **72** 051401
- [17] Yudin G L, Bandrauk A D and Corkum P B 2006 *Phys. Rev. Lett.* **96** 063002
- [18] Schultze M, Goulielmakis E, Uiberacker M, Hofstetter M, Kim J, Kim D, Krausz F and Kleineberg U 2007 *New J. Phys.* **9** 243
- [19] Graf U *et al* 2008 Intense few-cycle light pulses in the deep ultraviolet (submitted)
- [20] Seel M and Domcke W 1991 *J. Chem. Phys.* **95** 7806–22
- [21] Kitzler M, Milosevic N, Scrinzi A, Krausz F and Brabec Th 2002 *Phys. Rev. Lett.* **88** 173904
- [22] Itatani J, Quéré F, Yudin G L, Ivanov M Yu, Krausz F and Corkum P B 2002 *Phys. Rev. Lett.* **88** 173903
- [23] Quéré F, Mairesse Y and Itatani J 2005 *J. Mod. Opt.* **52** 339–60

- [24] Kosik E M, Corner L, Wyatt A S, Cormier E, Walmsley I A and DiMauro L F 2005 *J. Mod. Opt.* **52** 361–78
- [25] Yakovlev V S, Bammer F and Scrinzi A 2005 *J. Mod. Opt.* **52** 395–410
- [26] Dyson F J 1949 *Phys. Rev.* **75** 1736–1755
Becker W, Lohr A and Kleber M 1997 *Phys. Rev. A* **56** 645–656
- [27] Kazansky A K and Kabachnik N M 2006 *J. Phys. B: At. Mol. Opt. Phys.* **39** 5173–86
- [28] Kazansky A K and Kabachnik N M 2007 *J. Phys. B: At. Mol. Opt. Phys.* **40** 3413–24
- [29] Sansone G *et al* 2006 *Science* **314** 443–5
- [30] Smirnova O, Spanner M and Ivanov M Yu 2006 *J. Phys. B: At. Mol. Opt. Phys.* **39** S323–39
Smirnova O, Mouritzen A S, Patchkovskii S and Ivanov M Yu 2007 *J. Phys. B: At. Mol. Opt. Phys.* **40** F197–206
- [31] Yudin G L, Chelkowski S and Bandrauk A D 2006 *J. Phys. B: At. Mol. Opt. Phys.* **39** L17–24
- [32] Yudin G L, Patchkovskii S and Bandrauk A D 2006 *J. Phys. B: At. Mol. Opt. Phys.* **39** 1537–46
- [33] Yudin G L, Patchkovskii S, Corkum P B and Bandrauk A D 2007 *J. Phys. B: At. Mol. Opt. Phys.* **40** F93–103
- Yudin G L, Patchkovskii S, Corkum P B and Bandrauk A D 2007 *J. Phys. B: At. Mol. Opt. Phys.* **40** 2223
- Yudin G L, Patchkovskii S and Bandrauk A D 2008 *J. Phys. B: At. Mol. Opt. Phys.* **41** 045602
- [34] Butth C and Santra R 2008 *Phys. Rev. A* **77** 013413
- [35] Huber K P and Herzberg G 1979 *Molecular Spectra and Molecular Structure* vol 4 (Constants of Diatomic Molecules, Princeton, NJ: Van Nostrand-Reinhold)
- [36] Chan W F, Cooper G and Brion C E 1993 *Chem. Phys.* **170** 111–21
- [37] Shi H and Easta A L L 2006 *J. Chem. Phys.* **125** 104311
- [38] Aközbek *et al* 2006 *New J. Phys.* **8** 177
- [39] de Vivie R and Peyerimhoff S D 1988 *J. Chem. Phys.* **89** 3028–43
- [40] Dixit S N and McKoy V 1985 *J. Chem. Phys.* **82** 3546–53
- [41] Hehre W J, Stewart R F and Pople J A 1969 *J. Chem. Phys.* **51** 2657–773
- [42] Buckingham A D, Orr B J and Sichel J M 1970 *Phil. Trans. R. Soc. Lond. A* **268** 147–57
- [43] Dixit S N, Lynch D L, McKoy V and Huo W M 1985 *Phys. Rev. A* **32** 1267–70